

Nonlinear memory functions capture and explain dynamical behaviours

Edgar Herrera-Delgado^{1,2}, James Briscoe¹, and Peter Sollich^{2,3}

¹The Francis Crick Institute, 1 Midland Rd, London NW1 1AT, UK

²Department of Mathematics, King's College London, Strand, London WC2R 2LS, UK

³Institut für Theoretische Physik, University of Göttingen, Friedrich-Hund-Platz 1, 37077 Göttingen, Germany

james.briscoe@crick.ac.uk
peter.sollich@uni-goettingen.de

Abstract

Mathematical approaches from dynamical systems theory are used in a range of fields. This includes biology where they are used to describe processes such as protein-protein interaction and gene regulatory networks. As such networks increase in size and complexity, detailed dynamical models become cumbersome, making them difficult to explore and decipher. This necessitates the application of simplifying and coarse graining techniques in order to derive explanatory insight. Here we demonstrate that Zwanzig-Mori projection methods can be used to arbitrarily reduce the dimensionality of dynamical networks while retaining their dynamical properties. We show that a systematic expansion around the quasi-steady state approximation allows an explicit solution for memory functions without prior knowledge of the dynamics. The approach not only preserves the same steady states but also replicates the transients of the original system. The method also correctly predicts the dynamics of multistable systems as well as networks producing sustained and damped oscillations. Applying the approach to a gene regulatory network from the vertebrate neural tube, a well characterised developmental transcriptional network, identifies features of the regulatory network responsible for its characteristic transient behaviour. Taken together, our analysis shows that this method is broadly applicable to multistable dynamical systems and offers a powerful and efficient approach for understanding their behaviour.

Introduction

In complex dynamical systems, comprising multiple interacting components, it can be difficult to identify causal mechanisms and to dissect the function of parts of a system. Nonlinearities and feedback complicate intuitive understanding and these difficulties increase with the size and complexity of a system. Examples include biological processes such as protein-protein interaction and gene regulatory networks [Davidson, 2010, Snider et al., 2015]. Mathematical models of these systems allow exploratory analysis and can provide insight but become less practical as system size grows. More importantly, the complexity can obscure the explanation for unexpected or emergent behaviours that originate in the dynamics of a system. For these reasons, a variety of approaches have been developed to reduce the complexity of models while preserving desired features of their behaviour. An important class of tools are dimensionality reduction techniques that coarse grain parts of a system [Rega and Troger, 2005, Schnoerr et al., 2017, Bronstein and Koepl, 2018].

The Zwanzig-Mori formalism provides an exact dimensionality reduction of a dynamical system based on a separation into an arbitrary “subnetwork”, the components of which are tracked explicitly, and a “bulk” containing the components that are replaced with “memory functions” [Nakajima, 1958, Zwanzig, 1961, Mori, 1965, Kawasaki and Gunton, 1973]. These functions describe how the current subnetwork state feeds back, through the activity of molecular species in the bulk, to affect the subnetwork at a later time. This approach, specifically its nonlinear version, was

originally developed for the dynamics of physical systems [Zwanzig, 2001], but later generalized by Chorin and coworkers [Chorin et al., 2000, Chorin et al., 2002], with related uses also in optimal course graining [Weinan et al., 2008]. A limitation, however, is that the memory functions are generally impossible to calculate in closed form [Chorin et al., 2000, Chorin et al., 2002]. Although approximate expressions can be derived in special cases [Chorin and Stinis, 2006, Stinis, 2006, Beck et al., 2009, Thomas et al., 2012, Gouasmi et al., 2017], this restricts the applicability of the formalism. One option is to expand the dynamical equations around a fixed point and derive memory functions from this approximation [Rubin et al., 2014, Bravi and Sollich, 2017], but for multistable or oscillatory systems the memory functions obtained in this way do not capture all the behaviours of a system.

To address this limitation, we develop a method, based on the formalism of [Chorin et al., 2000], that allows the calculation of memory functions for generic dynamical systems without prior knowledge of the dynamics. We make one assumption: the bulk must not generate fixed points beyond those of the subnetwork, more specifically it must have a unique steady state for any subnetwork state, such as in [Gouasmi et al., 2017]. This is a natural condition: the subnetwork must be able to produce all fixed points itself, otherwise coarse graining cannot succeed. As the starting point for the dimensionality reduced dynamics we use the Quasi-steady state (QSS) approximation, where the bulk is always in steady state with the current subnetwork state as has been used in other contexts [Kang et al., 2019]. Memory functions are then constructed to correct the projected subnetwork state, by accounting for departures of the bulk

from its steady state. Our main technical result is an explicit solution for the functions capturing these memory effects, derived in a systematic expansion around the QSS approximation. We demonstrate that the approach accurately predicts the dynamics of systems that produce multiple steady states and even sustained or damped oscillations. We also illustrate its use by applying it to a gene regulatory network from the embryonic vertebrate neural tube [Cohen et al., 2014]. This is a transcriptional network of four interacting transcription factors with well described transient dynamics. We show how the memory functions generated by this approach provide insight into the features of the regulatory network that produce this transient behaviour. Taken together, the analysis introduces a broadly applicable method for the investigation and analysis of complex dynamical systems.

Mathematical derivation

Initial definitions

Following [Chorin et al., 2000], we start from a system with degrees of freedom \mathbf{x} evolving deterministically in time according to some nonlinear functions \mathbf{R} :

$$\frac{d\mathbf{x}}{dt} = \mathbf{R}(\mathbf{x}) \quad [1]$$

We define the “flow” $\phi(\mathbf{x}, t)$ as the state the system reaches at time t if it starts in some initial state \mathbf{x} ; this function thus obeys $\phi(\mathbf{x}, 0) = \mathbf{x}$ and $\frac{\partial}{\partial t}\phi(\mathbf{x}, t) = \mathbf{R}(\phi(\mathbf{x}, t))$. We want to understand the dynamics of some chosen set of observables that we denote by the vector \mathbf{A} . Such observables are functions of the state of the system, which we write as $\mathbf{A}(\mathbf{x})$. By analogy with the definition of ϕ , the time-dependent observables are then taken as

$$\mathbf{A}(\mathbf{x}, t) = \mathbf{A}(\phi(\mathbf{x}, t)) \quad [2]$$

so that $\mathbf{A}(\mathbf{x}, t)$ gives the value of the observables at time t if the system was initially in state \mathbf{x} . The resulting time evolution of the observables can again be described by a differential equation

$$\frac{\partial}{\partial t}\mathbf{A} = L\mathbf{A}(\mathbf{x}), \quad L = \sum_i R_i(\mathbf{x}) \frac{\partial}{\partial x_i} \quad [3]$$

with the Liouvillian L , a linear differential operator. The general setup above requires us to track the full \mathbf{x} -dependence of the chosen observables $\mathbf{A}(\mathbf{x}, t)$. To achieve a reduction in dimensionality, Chorin [Chorin et al., 2000] assumes that the \mathbf{x} are determined by \mathbf{A} at least statistically, i.e. have some probability distribution that (only) depends on the current \mathbf{A} . Averages (expectations) over this distribution are written as $E[\cdot|\mathbf{A}]$, and the average evolution of \mathbf{A} is governed by $\mathbf{v}(\mathbf{A}) = E[L\mathbf{A}(\cdot)|\mathbf{A}]$. Chorin [Chorin et al., 2000, Chorin et al., 2002] showed that the corrections to this in the actual time evolution take the form of a memory term and a so-called random force \mathbf{r} , giving the general form for the time evolution of \mathbf{A} as:

$$\frac{d}{dt}\mathbf{A} = \mathbf{v}(\mathbf{A}) + \int_0^t dt' \mathbf{M}(\mathbf{A}(t'), t - t') + \mathbf{r} \quad [4]$$

The memory function $\mathbf{M}(\mathbf{A}(t'), t - t')$ depends on time difference $\tau = t - t'$ and – nonlinearly – on the past observable

value $\mathbf{A}(t')$. Its evolution with τ is governed by the *deviations* of the drift from $\mathbf{v}(\mathbf{A})$; this evolution reads for a general observable $g(\mathbf{x}, \tau)$

$$\frac{\partial}{\partial \tau}g(\mathbf{x}, \tau) = Lg(\mathbf{x}, \tau) - E[(Lg)(\cdot, \tau)|\mathbf{A}(\mathbf{x})] \quad [5]$$

The memory function is obtained from the observable that measures exactly such fluctuations in the drift of the observables \mathbf{A} ,

$$\mathbf{F}(\mathbf{x}) = (L\mathbf{A})(\mathbf{x}) - E[L\mathbf{A}(\cdot)|\mathbf{A}(\mathbf{x})] \quad [6]$$

From $\mathbf{F}(\mathbf{x})$ we define an $\mathbf{F}(\mathbf{x}, \tau)$ [5] from the initial condition $\mathbf{F}(\mathbf{x}, 0) = \mathbf{F}(\mathbf{x})$, and the memory function is then given explicitly as $\mathbf{M}(\mathbf{A}, \tau) = E[L\mathbf{F}(\cdot, \tau)|\mathbf{A}]$. The random force itself is $\mathbf{r}(\mathbf{x}, t) = \mathbf{F}(\mathbf{x}, t)$ and has a vanishing average at all times, $E[\mathbf{r}(\cdot, t)|\mathbf{A}] = 0$ [Chorin et al., 2000]. We will drop this term in the following as the random force vanishes when the bulk starts in QSS. While in [Chorin et al., 2000] steady state dynamics are discussed, this is not required for the above formalism to be applicable.

Subnetwork dynamics

With the random force discarded as above, [4] is a closed equation for the time evolution of the observables \mathbf{A} and so achieves the desired dimensionality reduction. However, the memory function cannot in general be calculated in any closed form. We now show that this *can* be done, within a systematic approximation, for subnetwork dynamics. By this we mean that we consider as the observables $\mathbf{A} = \mathbf{x}^s$ a subset of \mathbf{x} , e.g. the concentrations of molecular species in a subnetwork of a large gene regulatory network. We denote the degrees of freedom in the rest of the network, the bulk, by \mathbf{x}^b and write out the components of the general time evolution [1] as

$$\frac{d\mathbf{x}^s}{dt} = \mathbf{R}^s(\mathbf{x}^s, \mathbf{x}^b), \quad \frac{d\mathbf{x}^b}{dt} = \mathbf{R}^b(\mathbf{x}^s, \mathbf{x}^b) \quad [7]$$

The Liouvillian then splits accordingly into

$$L = \sum_s R_s(\mathbf{x}^s, \mathbf{x}^b) \frac{\partial}{\partial x_s} + \sum_b R_b(\mathbf{x}^s, \mathbf{x}^b) \frac{\partial}{\partial x_b} \quad [8]$$

with the sums running over subnetwork and bulk species, respectively. Here and below subscripts always indicate individual species, while vectors with ‘s’ and ‘b’ superscripts collect all subnetwork and bulk quantities, respectively. With [8] the generic observable time evolution [3] $(\partial/\partial t)\mathbf{x}^s = L\mathbf{x}^s$ reduces to [7] as it should. We now need to choose how to define the expectation $E[\cdot|\mathbf{x}^s]$. We do this so that without the memory kernel, the reduced equation [4] corresponds to the simplification where the bulk dynamics equilibrates rapidly to any prevailing subnetwork state \mathbf{x}^s , reaching a quasi steady state (QSS) value \mathbf{x}^{b*} defined by $d\mathbf{x}^b/dt = 0$ or

$$\mathbf{R}^b(\mathbf{x}^s, \mathbf{x}^{b*}(\mathbf{x}^s)) = 0 \quad [9]$$

As motivated in the introduction we will assume that this condition determines a unique bulk QSS $\mathbf{x}^{b*}(\mathbf{x}^s)$ for any \mathbf{x}^s . The expectation required to construct the reduced equation [4] is taken accordingly as

$$E[g(\cdot)|\mathbf{x}^s] = g(\mathbf{x}^s, \mathbf{x}^{b*}(\mathbf{x}^s)) \quad [10]$$

i.e. by taking \mathbf{x}^s as prescribed and inserting for \mathbf{x}^b its QSS value. The average drift $\mathbf{v}(\mathbf{A}) = E[LA(\cdot)|\mathbf{A}] = E[\mathbf{R}^s(\mathbf{x}^s, \mathbf{x}^b)|\mathbf{x}^s]$ now evaluates directly from [10] as

$$\mathbf{v}(\mathbf{x}^s) = \mathbf{R}^s(\mathbf{x}^s, \mathbf{x}^{b*}(\mathbf{x}^s)) \quad [11]$$

This is the QSS or ‘fast bulk’ approximation to the subnetwork dynamics. Our main interest in the following lies in understanding the memory effects that account for the fact that the bulk is not in general fast, but evolves on a timescale comparable to that of the subnetwork. To determine the resulting memory function, we start from the definition of $F(\mathbf{x})$, which from [6] has components

$$F_s(\mathbf{x}^s, \mathbf{x}^b) = R_s(\mathbf{x}^s, \mathbf{x}^b) - R_s(\mathbf{x}^s, \mathbf{x}^{b*}(\mathbf{x}^s)) \quad [12]$$

The main challenge is now to calculate the evolution of this observable in time according to [5]. This is not feasible in general but we can develop a systematic approximation by *linearising* in deviations of the bulk degrees of freedom from the QSS, which we write as

$$F_s(\mathbf{x}^s, \mathbf{x}^b, \tau) \approx \sum_b (x_b - x_b^*(\mathbf{x}^s)) f_{bs}(\mathbf{x}^s, \tau) \quad [13]$$

The problem then reduces to finding the evolution of $f_{bs}(\mathbf{x}^s, \tau)$ from the initial condition $f_{bs}(\mathbf{x}^s, 0) \equiv f_{bs}^0(\mathbf{x}^s)$ obtained by linearising [12]:

$$f_{bs}^0(\mathbf{x}^s) = \frac{\partial R_s}{\partial x_b} \quad [14]$$

where the derivatives here and below are evaluated at $(\mathbf{x}^s, \mathbf{x}^{b*}(\mathbf{x}^s))$ unless otherwise specified.

Memory evolution over time

To derive our memory function we insert [13] into [5]. Consistently applying the linearisation as detailed in Supp. A yields the following equation for f_{bs} :

$$\frac{\partial}{\partial \tau} f_{bs} = \sum_{b'} l_{bb'} f_{b's} + \sum_{s'} R_{s'} \frac{\partial}{\partial x_{s'}} f_{bs} \quad [15]$$

with

$$l_{bb'} = J_{b'b} + \sum_{s'b''} (\mathbf{J}^{-1})_{b'b''} \frac{\partial R_{b''}}{\partial x_{s'}} \frac{\partial R_{s'}}{\partial x_b} \quad [16]$$

where the Jacobian matrix \mathbf{J} is defined as

$$J_{b''b'} = \frac{\partial R_{b''}}{\partial x_{b'}} \quad [17]$$

The next step is to find a solution $f_{bs}(\mathbf{x}^s, \tau)$ for the partial differential equation [15]. This can be done using the method of characteristics as the equation is linear in $f_{bs}(\mathbf{x}^s, \tau)$ and only involves first derivatives, and gives the closed form solution (see Supp. B)

$$f_{bs}(\mathbf{x}^s, \tau) = \sum_{b'} E_{bb'}(\tau) f_{b's}^0(\phi_v(\mathbf{x}^s, \tau)) \quad [18]$$

Here the $E_{bb'}$ are elements of the time-ordered matrix exponential $\mathbf{E}(\tau) = \exp[\int_0^\tau d\tau' \mathbf{l}(\phi_v(\mathbf{x}^s, \tau'))]$, and the propagation in time is performed with the flow ϕ_v for the QSS drift $\mathbf{v}(\mathbf{x}^s)$.

Memory function

We can now finally determine the memory function on subnetwork species s , which from the general framework set out above is

$$M_s(\mathbf{x}^s, \tau) = E[LF_s(\cdot, \tau)|\mathbf{x}^s] \quad [19]$$

We insert the expansion [13] here and obtain after some algebra (see Supp. A) our main result, a simple expression for the memory function:

$$M_s(\mathbf{x}^s, \tau) = \sum_{b'} c_{b'}(\mathbf{x}^s) f_{b's}(\mathbf{x}^s, \tau) \quad [20]$$

where we have denoted

$$c_{b'}(\mathbf{x}^s) = \sum_{s'} \sum_{b''} (\mathbf{J}^{-1})_{b'b''} \frac{\partial R_{b''}}{\partial x_{s'}} R_{s'} \quad [21]$$

These functions can be thought of as prefactors to the memory term. The general projected time evolution equation now takes the form

$$\frac{d}{dt} x_s = v_s(\mathbf{x}^s(t)) + \int_0^t dt' M_s(\mathbf{x}^s(t'), t - t') \quad [22]$$

The first term contains the QSS drift while the second one represents the memory correction to this, which is expressed in terms of the memory function [20]. Our derivation allows this memory to cover the behaviour around multiple fixed points of the system, due to its nonlinear dependence on \mathbf{x}^s . The interpretation of our result [20] is that in a small time interval dt' , $x_b - x_b^*$ will change by $c(\mathbf{x}^s(t')) dt'$. This deviation from the QSS is propagated by the exponential matrix and affects the drift R_s at time t as captured by f_{bs}^0 in [18]. In Supp. H we compare [20] with the work of [Gouasmi et al., 2017], which instead of the QSS assumption takes $\mathbf{x}^b = 0$. This is unsuitable for the multistable systems we are interested in but we show that the method can be adapted to project to bulk QSS values (Supp. I). This leads to an expression similar to [20], but crucially without the propagation in time from t' to $t = t' + \tau$ (Fig. S3).

Self-consistent approximation

Our linearisation approach [13] implies that the memory term captures dynamical effects that are of first order in the deviations of the bulk network from its QSS. We will now develop an approximate self-consistent way of incorporating higher order corrections, which turns out also to simplify the numerical evaluation of the memory terms. Consider the factor $f_{bs}^0(\phi_v(\mathbf{x}^s, \tau))$ that from [18,20] appears in the memory function $M_s(\mathbf{x}^s, \tau)$. In the actual memory integral this is evaluated for $\mathbf{x}^s(t')$ and $\tau = t - t'$, i.e. as $f_{bs}^0(\phi_v(\mathbf{x}^s(t'), t - t'))$. As explained above, ϕ_v is the flow generated only by the QSS drift, i.e. without memory corrections. But the memory terms change the flow, so we can make the approach self-consistent by substituting for ϕ_v the actual time evolution *with* memory. This corresponds to replacing

$$\phi_v(\mathbf{x}^s(t'), t - t') \rightarrow \mathbf{x}^s(t) \quad [23]$$

as we are just propagating the subnetwork state from $\mathbf{x}^s(t')$ by a time difference $t - t'$ to $\mathbf{x}^s(t)$. Making this replacement also in the matrix exponential in [18] changes the memory

term $\mathcal{M}_s(t) = \int_0^t dt' M_s(\mathbf{x}^s(t'), t - t')$ into

$$\tilde{\mathcal{M}}_s(t) = \sum_{b''} \int_0^t dt' \sum_{b'} c_{b'}(\mathbf{x}^s(t')) \left(e^{\int_{t'}^t dt'' \mathbf{v}(\mathbf{x}^s(t''))} \right)_{b'b''} \times f_{b''s}^0(\mathbf{x}^s(t)) \quad [24]$$

The dependence on the subnetwork species s on which the memory acts is contained only in the – now t' -independent – factor $f_{b''s}^0(\mathbf{x}^s(t'))$. As shown in Supp. C, the memory integrals in the first line can then be calculated efficiently as solutions to differential equations, one for each bulk species b'' . Conceptually, however, the self-consistent memory term is more complicated. In the original formulation [22], the memory is a superposition of separate effects from all past times t' : the state $\mathbf{x}^s(t')$ of the subnetwork affects the behaviour of the bulk and feeds back into the subnetwork at time t . In [24], the way this feedback acts is additionally modulated by the entire time evolution of the subnetwork between times t' and t . In the applications considered below both approaches yield similar quantitative results, hence which one to choose depends on the aim: for numerical calculations of memory effects the self-consistent version is more efficient, whereas the memory functions themselves are easier to analyse in the original version because they depend – in addition to time difference, which always features – only on the subnetwork state at one time t' .

Memory decomposition

As in [Herrera-Delgado et al., 2018] it is possible to decompose the memory into specific channels in order to analyse the contribution of interactions within a network. We take advantage of the two partial derivative expressions in [14, 21] to decompose the memory exactly into combinations of incoming and outgoing channels (Supp. D). The analogous construction for the self-consistent approximation is set out in Supp. E.

Applications

To test the effectiveness of the method we examine systems that contain multiple steady states, oscillatory behaviours and complex transient dynamics. These are relevant in a wide range of physical and biological contexts.

Multistability

We first examine a series of multistable systems defined by mutually repressive Hill functions:

$$\frac{d}{dt} x_j = \frac{a}{1 + \sum_{i \neq j} x_i^n} - x_j \quad [25]$$

The above equation constitutes an “or” logic because of the sum of the terms in the denominator, where even if only one repressor has a high concentration, the production rate will become very low. These kinds of interaction lead to multistability in a wide variety of developmental systems [Angeli et al., 2004].

We test the method on the simplest case with two nodes $\{x_1, x_2\}$. We place x_2 in the bulk and calculate the memory function for the single remaining subnetwork species x_1 . This depends on the past concentration $x_1(t')$ and the time

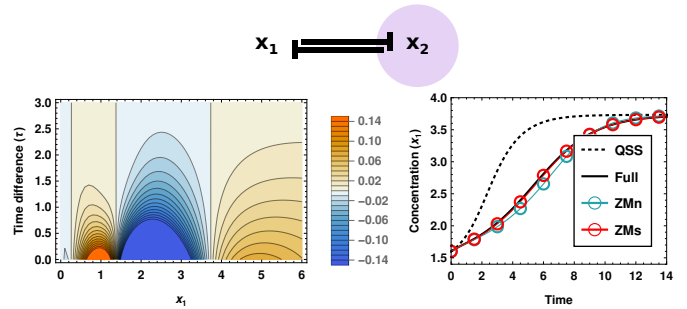


Figure 1: (Top) Network illustrating a bistable switch defined using cross-repressive Hill functions [25] with $a = 4$, $n = 2$. For this and all other network illustrations, blunt arrows indicate repression; purple shading identifies the species placed in the bulk. (Left) Memory function for the bistable switch shown as a function of (past) concentration x_1 of species 1 (x -axis) and time difference τ (y -axis) running from present and past. Memory function values range from negative to positive as indicated by the scale bar on the right, and are capped by blue and orange outside the scale bar range. (Right) Time course of the system demonstrates the capacity of both the nonlinear (ZMn; cyan) and self-consistent (ZMs; red) projections to capture the timescale and shape of transients of the full model (solid line) in reaching a stable fixed point. The QSS approximation (dashed line) significantly underestimates the length of the transient, showing that the ZM projections successfully correct for x_2 not being at QSS.

difference $\tau = t - t'$ (Fig. 1). We observe that the memory becomes zero at each fixed point as expected from [Herrera-Delgado et al., 2018], where the memory was obtained as an expansion (to quadratic order) in deviations of \mathbf{x}^s from a fixed point. To leading order the memory grows linearly with this deviation, and in line with this we see it changing sign at every fixed point. The sign of the memory in all cases is opposite to that of the drift, so the memory delays the relaxation time to the corresponding steady state. This makes intuitive sense as in the original system, the bulk species’ state reacts relatively slowly to subnetwork changes, rather than infinitely fast as the QSS approximation assumes.

To test the accuracy of our method in capturing the transient temporal dynamics we set the initial condition of x_1 to be close to the unstable fixed point of the QSS dynamics; here we are furthest from the stable fixed points and so can test the limits of the method. As a ground truth baseline we choose the full dynamics of the original system, setting x_2 at time zero to its QSS value with respect to the value of x_1 . We compare this to the subnetwork dynamics predicted by the simple QSS dynamics, and by our approach, which includes memory corrections. For this example we evaluate both the nonlinear memory description [22], which we label ZMn (Zwanzig-Mori nonlinear), and the self-consistent memory [24], denoted ZMs (Zwanzig-Mori self-consistent) below. We find that both replicate the behaviour of the original system well, independently of whether the initial condition eventually leads to the low- or high- x_1 fixed point. The QSS approximation, on the other hand, reaches the steady state unrealistically fast (Fig. 1). Given that the ZMs is substantially easier to implement for time course prediction (Supp. C) we concentrate on this approach below. Further justification for this comes from the fact that

the self-consistent memory description is *exact* when R^s and R^b depend at most linearly on the bulk species, as we show in Supp. F. This exactness is not a trivial consequence of the fact that our approach is a linearisation in $x^b - x^{b*}$, as it would otherwise hold also in the ZMn version. Systems with linear x^b -dependences usually involve mass-action reactions and can produce bistable systems or oscillations [Wilhelm, 2009, Kondepudi and Prigogine, 1998], which we can then reproduce exactly with the ZMs projection (see Figs. S1, S2).

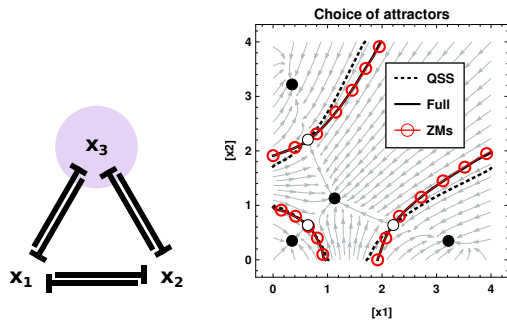


Figure 2: (Left) Network illustrating the cross-repressive tetrastable system [25]; purple shading indicates the species placed in the bulk. (Right) Phase portrait indicating the basins of attraction of the four stable fixed points (black circles) and the unstable fixed points (white circles). The separatrices bounding each basin are shown for the full dynamics (solid lines), QSS approximation (dotted lines) and the sub-network equations with memory (ZMs, red circles); stream plots are shown for the QSS approximation. The QSS approach shows a clear difference to the original system, while the boundaries set by ZMs and the full system are almost indistinguishable.

We next tested the approach on a tetrastable system defined in the same way as [25] with variables $\{x_1, x_2, x_3\}$. We consider the subnetwork containing x_1 and x_2 , which will allow us to investigate the effect of the memory effects on the shapes of the basins of attraction of the different (stable) fixed points. For the parameter values we use, there are four such fixed points for the full network: three where only one species has high concentration and the other two low, and one where all concentrations are equal (Fig. 2). The boundaries of the basins of attraction can be viewed as the points where fate decisions of the system change. We find that the QSS system fails to replicate the decision process of the original system, whereas the ZMs accurately identifies both the eventual steady state (Fig. 2) *and* the timing to get to this state (data not shown).

Oscillations

We further explore the ability of the subnetwork equations with memory to reproduce oscillations arising from a unidirectional repressive network. We use the repressilator system [Elowitz and Leibler, 2000], with variables $\{x_1, x_2, x_3\}$ and repressive interactions as shown in Fig. 3 and represented mathematically by

$$\frac{d}{dt}x_j = \frac{a}{1 + x_{j-1}^n} - x_j \quad [26]$$

where $x_0 \equiv x_3$. We first compare the bifurcation diagram that results from varying both system parameters a and n , in

order to see whether the subnetwork equations with memory can replicate the 2D Hopf bifurcation of the original system, from damped to sustained oscillations (Fig. 3).

In contrast to the QSS approximation we find that the projection technique correctly replicates the existence of sustained oscillations and predicts a qualitatively correct bifurcation diagram. The period and amplitude of sustained oscillations in the relevant parameter regime is less well replicated (not shown). For damped oscillations the subnetwork equations with memory work accurately in predicting the full temporal dynamics (Fig. 4). By contrast, the QSS approximation displays almost no oscillatory behaviour and none of a sustained nature, highlighting the importance of memory effects for oscillatory transients.

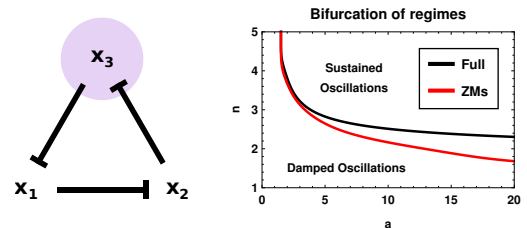


Figure 3: (Left) Network illustrating the repressilator system [26]; purple shading indicates the species placed in the bulk. (Right) Bifurcation diagram of the repressilator for system parameters a and n . The lines represent super-critical Hopf bifurcations. The QSS system can only produce damped oscillations, so has no bifurcation at all. The ZMs system (red line) shows a good qualitative match to the shape and position of the bifurcation of the full system (solid black line).

In order to understand in more detail how memory generates oscillations, we analyse the corresponding memory functions. We first plot the memory amplitude, i.e. the value $M(x^s, 0)$ for memory from the immediate past ($t' = t$) across the configuration space of our subnetwork (Fig. 4 right) and observe two distinct regions with positive and negative memory amplitude, separated by a line where this amplitude vanishes (black). Plotting the time course from Fig. 4 left in the same representation we observe that it crosses the black line many times. The corresponding changes in the sign of the memory amplitude are what drives the oscillations seen in Fig. 4 left.

Neural tube network (transients and multistability)

Finally we apply the projection approach to a biologically relevant system with several bifurcations and non-trivial dynamical properties, specifically the neural tube network described in [Cohen et al., 2014] (Fig. 5). This is in fact a family of networks varying with neural tube position, parametrised below in terms of p running from 0 to 1. As a first approach, similarly to how we proceeded in [Herrera-Delgado et al., 2018], we place Nkx2.2 and Olig2 in the subnetwork given that these two alone generate a bistable switch, so the remaining bulk behaviour is now provided by the two other species (Irx3 and Pax6).

We test the method at the position along the neural tube where the model has the most complexity, a region of trista-

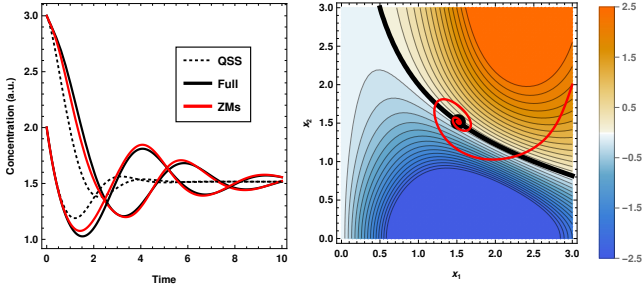


Figure 4: (Left) Damped oscillations generated by the repressilator [Elowitz and Leibler, 2000] can be accurately reproduced by the projection approach (red line) while the QSS (dotted line) fails to replicate both the timing and the amplitude of the oscillations of the full system (solid black line). (Right) Colour map of memory amplitude (memory at $\tau = 0$) as a function of (x_1, x_2) . The memory amplitude changes from negative (blue) to positive (orange) across the thick black line. Red curve: Parametric plot of the ZMs time course from the left; the memory repeatedly changes from negative to positive to drive the correct oscillations.

bility ($p = 0.65$), and compare with the original system and the QSS approximation (Fig. 5). We find that as for the tetrastable case (Fig. 2), the projection accurately replicates the choice of steady state, in contrast to the QSS method (Fig. 5). Importantly we find that memory forces the system to pass through a pMN region when transitioning between p2 and p3 fates; this qualitative feature is lost in the QSS approximation. At other neural tube positions we also consistently find a good match between the original system and the ZMs projection approach (not shown).

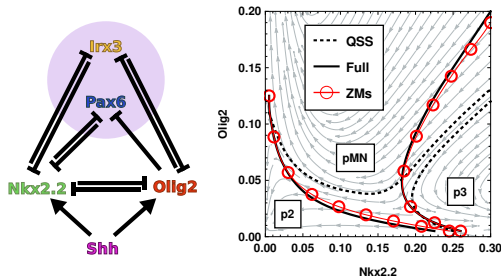


Figure 5: (Left) Neural tube network [Cohen et al., 2014] defined by cross-repressive interactions between four transcription factors and activation by Sonic Hedgehog signalling (Shh); purple shading indicates choice of bulk. (Right) Fate decision diagram for a neural tube position with three attractors (at position $p = 0.65$); solid lines indicate boundaries between different fate choices. Possible steady states are p3 (high Nkx2.2, right), pMN (high Olig2, top) and p2 (low Nkx2.2 & Olig2, and high Irx3 & Pax6, bottom left). Dashed lines indicate basin boundaries for the QSS approximation and red dots the basin boundaries for the ZMs projection; a stream plot is shown for the QSS system. The ZMs system very accurately reproduces the boundaries of the full system.

We next analyse the temporal evolution of the systems at various neural tube positions, using the experimentally determined initial condition for Nkx2.2 and Olig2 of zero; we again compare the ZMs description with the original system and the QSS reduction. The ZMs predictions show a good

fit with the original system at all positions (Fig. 6 displays results for a position with a strongly non-monotonic transient, $p = 0.1$), demonstrating that the memory functions are capable of accurately capturing not just final cell fate decisions but also the timing of such decisions. This temporal aspect is important for correct patterning as explored in [Exelby et al., 2019].

Decomposing nonlinear memory functions

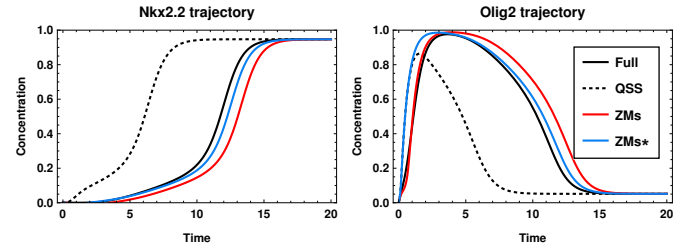


Figure 6: Time courses of concentrations of Nkx2.2 (left) and Olig2 (right) in p3 domain ($p = 0.1$). A transient expression of Olig2 leading to a delay in Nkx2.2 expression is observed *in vivo*. The full system (solid line) and ZMs projections (with Nkx2.2 and Olig2 chosen as subnetwork, see Fig. 5, red and blue) qualitatively reproduce this behaviour. In contrast, the QSS approximation (dashed line) is unable to capture the long Olig2 transient. ZMs* represents the removal of all memory functions except those specified in Fig. 7, which suffice to capture the observed transient.

In order to understand how memory functions affect the patterning dynamics, we set out to understand their structure. We perform our self-consistent memory decomposition approach (Supp. E) and analyse the results to identify the memory channels with the most impact on the time courses based on their contribution along the trajectory (Fig. S5). Performing this analysis for the different progenitor domains predicts the most important regulatory interactions contributing to the memory effect at each neural tube position (Fig. 7). This indicates marked differences in the most significant memory channels at different neural tube positions (see Fig. S5 for an illustration of the decomposition in the p3 domain at $p = 0.1$).

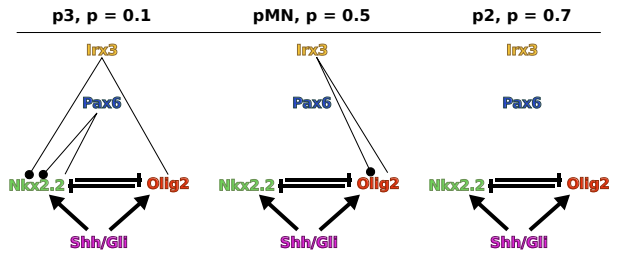


Figure 7: Diagrams indicating the channels that have the largest memory contributions to the observed dynamics at three distinct neural tube positions. Black dot indicates the species receiving the memory contribution; the other end of each line is the species “sending” the memory. Contributions change according to the final steady state: p3 (left), pMN (centre) and p2 (right).

To test the validity of our results we remove all channels identified as unimportant, setting them to QSS, thereby

keeping only the channels shown in Fig. 7. Simulating the dynamics with only these memory functions results in dynamics that match closely those of the full simulation (Fig. 6), confirming the prediction that these channels dominate the memory effects.

We next investigated the experimentally validated transient in gene expression in the p3 domain (monostable with high Nkx2.2 in the steady state, $p = 0.1$, Fig. 6). Nkx2.2 induction is delayed in neural progenitor cells compared to Olig2 [Dessaud et al., 2007] and our analysis of the memory function provides insight into how this is achieved. The active memory channels ensure that Nkx2.2 is kept close to zero while Olig2 rises (Fig. 6). The dominant memory channels shown in Fig. 7 (left) indicate that a different bulk species captures the history of each subnetwork species: Pax6 transmits the memory of Nkx2.2 and Irx3 the one of Olig2. The effect of these these bulk species is thus to delay Nkx2.2 expression based on the past expression of Nkx2.2 and Olig2.

Finally, we examined whether the effect of the two memory functions (one for Olig2 and one for Nkx2.2) that reflect the influence of the bulk is to increase the robustness of the system to initial conditions. For the system with memory, the delay in Nkx2.2 expression is present for multiple initial conditions, with trajectories crossing in a way that would be impossible to reproduce with a memoryless system (Fig. 8). From Fig. 7, the memory has two dominant channels reacting to changes in Nkx2.2 and Olig2, respectively. This ensures that if even one of the subnetwork species levels drifts away from zero, the memory pushes the path back into the “correct” direction. In the case of the memoryless system, the already short transient observed in Fig. 6 disappears completely as soon as the initial conditions are no longer zero for Nkx2.2 (Fig. 8). In general a transient is difficult to achieve in a 2D memoryless system where a very specific function would have to repress Nkx2.2 at both low and medium-high levels of Olig2. We find that the memory generated by the combination of Pax6 and Irx3 provides robustness to changes in initial condition as the memory leads to low levels of Nkx2.2 during the initial phases of the transient (Fig. 8)

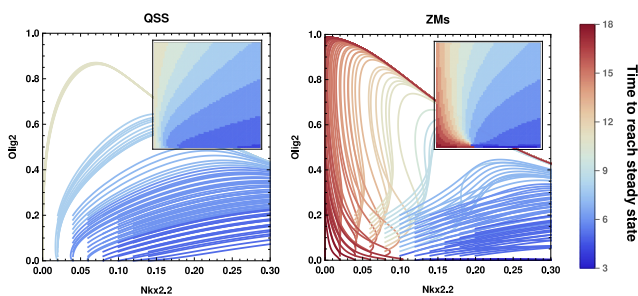


Figure 8: Trajectories from multiple initial conditions starting near zero for Olig2 and Nkx2.2 in the p3 region ($p = 0.1$). The comparison emphasises the robustness provided by the memory functions (ZMs, right) in comparison to a memoryless system (QSS, left). All trajectories reach the same attractor with high Nkx2.2 and low Olig2. The ZMs system behaves almost identically to the full system, with transient increases in Olig2 and large delays in reaching the steady state from a variety of initial conditions. Colour indicates time taken to reach final steady state, quantified as Nkx2.2 deviating less than 1% from its asymptotic concentration. Insets have same axes as main plots and show time to final steady state from a given initial position.

Summary

We have developed a version of the Zwanzig-Mori formalism, building on the work of Chorin and colleagues [Chorin et al., 2000], to obtain closed-form memory functions that can be used to reduce the dimensionality of a dynamical system far from equilibrium. We have demonstrated the accuracy of the approach in capturing emergent dynamics such as non-trivial transients and sustained or damped oscillations. By construction the method can capture multistability and we have shown its accuracy in predicting the basins of attraction that delineate cell fate decisions. We subsequently applied the method to a biologically relevant system, the neural tube patterning network [Cohen et al., 2014]. The reduced model captures the dynamics of the original system through non-monotonic transients. In addition it provides a novel understanding of the cause of such transients in gene expression and suggests that memory effects, stored in independent bulk nodes, provide robustness to initial conditions. We have demonstrated the generality of this method and its flexibility and applicability to dynamical systems.

Materials and methods

The equations and corresponding parameters are either stated or given in the original articles cited.

Acknowledgements

We thank Matthias Fuchs and Alberto Pezzotta for helpful discussions and comments on the manuscript. This work was supported by: the Francis Crick Institute, which receives its core funding from Cancer Research UK (FC001051), the UK Medical Research Council (FC001051), and Wellcome (FC001051); funding from Wellcome [WT098325MA and WT098326MA]; the European Research Council under European Union (EU) Horizon 2020 research and innovation program grant 742138.

References

- [Angeli et al., 2004] Angeli, D., Ferrell, J. E., and Sontag, E. D. (2004). Detection of multistability, bifurcations, and hysteresis in a large class of biological positive-feedback systems. *Proceedings of the National Academy of Sciences*, 101(7):1822–1827.
- [Beck et al., 2009] Beck, C. L., Lall, S., Liang, T., and West, M. (2009). Model reduction, optimal prediction, and the Mori-Zwanzig representation of Markov chains. *Proceedings of the IEEE Conference on Decision and Control*, pages 3282–3287.
- [Bravi and Sollich, 2017] Bravi, B. and Sollich, P. (2017). Inference for dynamics of continuous variables: The extended Plefka expansion with hidden nodes. *Journal of Statistical Mechanics: Theory and Experiment*, 2017(6):063404.
- [Bronstein and Koepl, 2018] Bronstein, L. and Koepl, H. (2018). Marginal process framework: A model reduc-

- tion tool for Markov jump processes. *Physical Review E*, 97(6):1–14.
- [Chorin et al., 2000] Chorin, A. J., Hald, O. H., and Kupferman, R. (2000). Optimal prediction and the Mori-Zwanzig representation of irreversible processes. *Proceedings of the National Academy of Sciences*, 97(7):2968–2973.
- [Chorin et al., 2002] Chorin, A. J., Hald, O. H., and Kupferman, R. (2002). Optimal prediction with memory. *Physica D: Nonlinear Phenomena*, 166(3-4):239–257.
- [Chorin and Stinis, 2006] Chorin, A. J. and Stinis, P. (2006). Problem reduction, renormalization, and memory. *Communications in Applied Mathematics and Computational Science*, 1(1):1–27.
- [Cohen et al., 2014] Cohen, M., Page, K. M., Perez-Carrasco, R., Barnes, C. P., and Briscoe, J. (2014). A theoretical framework for the regulation of Shh morphogen-controlled gene expression. *Development*, 141(20):3868–3878.
- [Davidson, 2010] Davidson, E. H. (2010). Emerging properties of animal gene regulatory networks. *Nature*, 468(7326):911–920.
- [Dessaud et al., 2007] Dessaud, E., Yang, L. L., Hill, K., Cox, B., Ulloa, F., Ribeiro, A., Mynett, A., Novitch, B. G., and Briscoe, J. (2007). Interpretation of the sonic hedgehog morphogen gradient by a temporal adaptation mechanism. *Nature*, 450(7170):717–720.
- [Elowitz and Leibier, 2000] Elowitz, M. B. and Leibier, S. (2000). A synthetic oscillatory network of transcriptional regulators. *Nature*, 403(6767):335–338.
- [Exelby et al., 2019] Exelby, K., Herrera-Delgado, E., Garcia Perez, L., Perez-Carrasco, R., Sagner, A., Metzis, V., Sollich, P., and Briscoe, J. (2019). Precision of Tissue Patterning is Controlled by Dynamical Properties of Gene Regulatory Networks. *bioRxiv*.
- [Gouasmi et al., 2017] Gouasmi, A., Parish, E. J., and Duraisamy, K. (2017). A priori estimation of memory effects in reduced-order models of nonlinear systems using the Mori-Zwanzig formalism. *Proceedings of the Royal Society A: Mathematical, Physical and Engineering Sciences*, 473(2205):20170385.
- [Herrera-Delgado et al., 2018] Herrera-Delgado, E., Perez-Carrasco, R., Briscoe, J., and Sollich, P. (2018). Memory functions reveal structural properties of gene regulatory networks. *PLoS Computational Biology*, 14(2):1–25.
- [John, 1978] John, F. (1978). *Partial Differential Equations*, volume 1 of *Applied Mathematical Sciences*. Springer US, New York, NY.
- [Kang et al., 2019] Kang, H. W., KhudaBukhsh, W. R., Koepl, H., and Rempała, G. A. (2019). Quasi-Steady-State Approximations Derived from the Stochastic Model of Enzyme Kinetics. *Bulletin of Mathematical Biology*, 81(5):1303–1336.
- [Kawasaki and Gunton, 1973] Kawasaki, K. and Gunton, J. D. (1973). Theory of nonlinear transport processes: Nonlinear shear viscosity and normal stress effects. *Physical Review A*, 8(4):2048–2064.
- [Kondepudi and Prigogine, 1998] Kondepudi, D. and Prigogine, I. (1998). *Modern Thermodynamics: From Heat Engines to Dissipative Structures*. John Wiley and Sons.
- [Mori, 1965] Mori, H. (1965). Transport, Collective Motion, and Brownian Motion. *Progress of Theoretical Physics*, 33(3):423–455.
- [Nakajima, 1958] Nakajima, S. (1958). On Quantum Theory of Transport Phenomena. *Progress of Theoretical Physics*, 20(6):948–959.
- [Rega and Troger, 2005] Rega, G. and Troger, H. (2005). Dimension Reduction of Dynamical Systems: Methods, Models, Applications. *Nonlinear Dynamics*, 41(1-3):1–15.
- [Rubin et al., 2014] Rubin, K. J., Lawler, K., Sollich, P., and Ng, T. (2014). Memory effects in biochemical networks as the natural counterpart of extrinsic noise. *Journal of Theoretical Biology*, 357:245–267.
- [Schoerr et al., 2017] Schoerr, D., Sanguinetti, G., and Grima, R. (2017). Approximation and inference methods for stochastic biochemical kinetics - A tutorial review. *Journal of Physics A: Mathematical and Theoretical*, 50(9):093001.
- [Snider et al., 2015] Snider, J., Kotlyar, M., Saraon, P., Yao, Z., Jurisica, I., and Stagljar, I. (2015). Fundamentals of protein interaction network mapping. *Molecular Systems Biology*, 11(12):848.
- [Stinis, 2006] Stinis, P. (2006). A comparative study of two stochastic mode reduction methods. *Physica D: Nonlinear Phenomena*, 213(2):197–213.
- [Thomas et al., 2012] Thomas, P., Grima, R., and Straube, A. V. (2012). Rigorous elimination of fast stochastic variables from the linear noise approximation using projection operators. *Physical Review E - Statistical, Nonlinear, and Soft Matter Physics*, 86(4):041110.
- [Weinan et al., 2008] Weinan, E., Li, T., and VandenEijnden, E. (2008). Optimal partition and effective dynamics of complex networks. *Proceedings of the National Academy of Sciences of the United States of America*, 105(23):7907–7912.
- [Wilhelm, 2009] Wilhelm, T. (2009). The smallest chemical reaction system with bistability. *BMC Systems Biology*, 3(1):90.
- [Zwanzig, 1961] Zwanzig, R. (1961). Memory effects in irreversible thermodynamics. *Physical Review*, 124(4):983–992.
- [Zwanzig, 2001] Zwanzig, R. (2001). *Nonequilibrium Statistical Mechanics*. Oxford University Press.

A Expansion around QSS

In this appendix we detail how we derive the memory evolution over time. We make use of our expansion [13] to find for the first term on the RHS of [5]

$$LF_s = \sum_b R_b(\mathbf{x}^s, \mathbf{x}^b) f_{bs}(\mathbf{x}^s, \tau) + \sum_{s'} R_{s'}(\mathbf{x}^s, \mathbf{x}^b) \sum_b (x_b - x_b^*) \frac{\partial}{\partial x_{s'}} f_{bs}(\mathbf{x}^s, \tau) - \sum_{s'} R_{s'}(\mathbf{x}^s, \mathbf{x}^b) \sum_b \frac{\partial x_b^*}{\partial x_{s'}} f_{bs}(\mathbf{x}^s, \tau) \quad [S1]$$

where the two last terms arise by differentiating the product $(x_b - x_b^*) f_{bs}(\mathbf{x}^s, \tau)$ w.r.t. $x_{s'}$ and we have not written the \mathbf{x}^s -dependence of \mathbf{x}^{b*} for brevity. The second term on the RHS of [5] is the expectation of this, obtained by replacing \mathbf{x}^b by \mathbf{x}^{b*} :

$$E[LF_s | \mathbf{x}^s] = \sum_b R_b(\mathbf{x}^s, \mathbf{x}^{b*}) f_{bs}(\mathbf{x}^s, \tau) - \sum_{s'} R_{s'}(\mathbf{x}^s, \mathbf{x}^{b*}) \sum_b \frac{\partial x_b^*}{\partial x_{s'}} f_{bs}(\mathbf{x}^s, \tau) \quad [S2]$$

Putting the two together gives for the time evolution [5] of F_s

$$\frac{\partial F_s}{\partial \tau} = \sum_b [R_b(\mathbf{x}^s, \mathbf{x}^b) - R_b(\mathbf{x}^s, \mathbf{x}^{b*})] f_{bs}(\mathbf{x}^s, \tau) + \sum_{s'} R_{s'}(\mathbf{x}^s, \mathbf{x}^b) \sum_b (x_b - x_b^*) \frac{\partial}{\partial x_{s'}} f_{bs}(\mathbf{x}^s, \tau) - \sum_{s'b} [R_{s'}(\mathbf{x}^s, \mathbf{x}^b) - R_{s'}(\mathbf{x}^s, \mathbf{x}^{b*})] \frac{\partial x_b^*}{\partial x_{s'}} f_{bs}(\mathbf{x}^s, \tau) \quad [S3]$$

For consistency with [13] we now linearise the square brackets again in $\mathbf{x}^b - \mathbf{x}^{b*}$. In the second term we similarly replace $R_{s'}(\mathbf{x}^s, \mathbf{x}^b)$ by $R_{s'}(\mathbf{x}^s, \mathbf{x}^{b*})$ as the remaining factor in this term is already linear. Comparing then with the time derivative of the original linearised formula [13] gives, after appropriate relabelling of indices, the equation the evolution of f_{bs} in time [15].

From the above expansion one sees that the matrix $l_{bb'}$ in [15] takes the form

$$l_{bb'} = \frac{\partial R_{b'}}{\partial x_b} - \sum_{s'} \frac{\partial R_{s'}}{\partial x_b} \frac{\partial x_{b'}^*}{\partial x_{s'}} \quad [S4]$$

The form [16] in the main text is the obtained by using the identity

$$\frac{\partial x_{b'}^*}{\partial x_{s'}} = - \sum_{b''} (\mathbf{J}^{-1})_{b'b''} \frac{\partial R_{b''}}{\partial x_{s'}} \quad [S5]$$

The latter can be obtained by differentiating [9] w.r.t. x_s .

To obtain the actual memory function from [19] is now straightforward as we have already worked out the required expectation in [S2]. The first term on the r.h.s. of [S2]., which we had previously kept to make the ensuing linearisation easier to see, actually vanishes because of [9], yielding

$$M_s(\mathbf{x}^s, \tau) = - \sum_{s'b'} R_{s'} \frac{\partial x_{b'}^*}{\partial x_{s'}} f_{b's}(\mathbf{x}^s, \tau) \quad [S6]$$

Using again the identity [S5] we obtain our main result [20].

B Solution for f

In this appendix we find the solution $f_{bs}(\mathbf{x}^s, \tau)$ to the differential equation [15]. We start by restating the latter as

$$\frac{\partial}{\partial \tau} f_{bs} - \sum_{s'} v_{s'}(\mathbf{x}^s) \frac{\partial}{\partial x_{s'}} f_{bs} = \sum_{b'} l_{bb'}(\mathbf{x}^s) f_{b's} \quad [S7]$$

where we have used that the factor $R_{s'}$ in [15] is just the effective drift $v_{s'}$ defined in [11]. As the equation is linear in f_{bs} and its derivatives it can be solved using the method of characteristics (see e.g. [John, 1978]). Calling the curve parameter for a characteristic u , the characteristic equations can be read off from [S7] as

$$\frac{d\tau}{du} = 1 \quad [S8]$$

$$\frac{dx_s}{du} = -v_s(\mathbf{x}^s) \quad [S9]$$

$$\frac{df_{bs}}{du} = \sum_{b'} l_{bb'}(\mathbf{x}^s) f_{b's} \quad [S10]$$

Setting an arbitrary integration constant to zero, the first of these gives $\tau = u$. To solve [S9] we call ϕ_v the flow generated by $v(\mathbf{x}^s)$, which is defined as the solution of the differential equation

$$\frac{\partial}{\partial \tau} \phi_v(\mathbf{x}^s, \tau) = v(\phi_v(\mathbf{x}^s, \tau)), \quad \phi_v(\mathbf{x}^s, 0) = \mathbf{x}^s \quad [\text{S11}]$$

The solution of [S9] is then

$$\mathbf{x}^s(u) = \phi_v(\mathbf{x}_0^s, -u) \quad [\text{S12}]$$

where \mathbf{x}_0^s is the value at the beginning of the characteristic curve ($u = 0$); the minus sign in the second argument of ϕ_v reflects the “backward in time” propagation in [S9]. We note for later that, as a consequence of [S12], the solution values at u_1 and u_2 are related by

$$\mathbf{x}^s(u_2) = \phi_v(\mathbf{x}^s(u_1), -u_2 + u_1) \quad [\text{S13}]$$

Finally, the solution of [S10] is

$$f_{bs}(u) = \sum_{b'} \left(e^{\int_0^u du' \mathbf{l}(\mathbf{x}^s(u'))} \right)_{bb'} f_{b's}^0(\mathbf{x}_0^s) \quad [\text{S14}]$$

using the initial condition [14] at $\tau = u = 0$. From [S10] we see that the matrix exponential appearing here must be time-ordered, with earlier “times” u' appearing to the right of later ones.

It now remains to express $f_{bs}(u)$ in terms of $\mathbf{x}^s(u)$ and $\tau(u) = u$. We fix a $\hat{u} = \hat{\tau}$ and call $\hat{\mathbf{x}}^s = \mathbf{x}^s(\hat{u})$. Using [S13] with $u_2 = u'$ and $u_1 = u$ then shows that the \mathbf{x}^s -solution [S12] can be expressed in terms of $\hat{\mathbf{x}}^s$ as

$$\mathbf{x}^s(u') = \phi_v(\hat{\mathbf{x}}^s, \hat{\tau} - u') \quad [\text{S15}]$$

and in particular $\mathbf{x}_0^s = \phi_v(\hat{\mathbf{x}}^s, \hat{\tau})$, so that

$$f_{bs}(\hat{\mathbf{x}}^s, \hat{\tau}) = \sum_{b'} \left(e^{\int_0^{\hat{\tau}} du' \mathbf{l}(\phi_v(\hat{\mathbf{x}}^s, \hat{\tau} - u'))} \right)_{bb'} f_{b's}^0(\phi_v(\hat{\mathbf{x}}^s, \hat{\tau})) \quad [\text{S16}]$$

Changing integration variable to $\tau' = \hat{\tau} - u'$ and dropping the hats then gives the solution [18] announced in the main text. Note that as $\tau' = \hat{\tau} - u'$, the time ordering of the matrix exponential

$$\mathbf{E}(\tau) = \exp \left(\int_0^\tau d\tau' \mathbf{l}(\phi_v(\mathbf{x}^s, \tau')) \right) \quad [\text{S17}]$$

is such that the earlier τ' are now on the *left*. The appropriate time ordered matrix exponential is defined formally via its Taylor series

$$\mathbf{E}(\tau) = \mathbf{1} + \sum_{n=1}^{\infty} \int \prod_{i=1}^n d\tau_i \mathbf{l}(\phi_v(\mathbf{x}^s, \tau_1)) \times \cdots \times \mathbf{l}(\phi_v(\mathbf{x}^s, \tau_n)) \quad [\text{S18}]$$

with $\mathbf{1}$ the identity matrix and the integration in the other terms running over the range $0 < \tau_1 < \dots < \tau_n < \tau$.

C Mapping of self-consistent memory to differential equations

We show in this appendix how to map the subnetwork equations with self-consistent memory,

$$\frac{\partial}{\partial t} x_s = v_s(\mathbf{x}^s(t)) + \tilde{\mathcal{M}}_s(t) \quad [\text{S19}]$$

to a set of differential equations. The self-consistent memory term $\tilde{\mathcal{M}}_s(t)$ is given by [24]

$$\tilde{\mathcal{M}}_s(t) = \sum_{b''} \int_0^t dt' \sum_{b'} c_{b'}(\mathbf{x}^s(t')) \left(e^{\int_{t'}^t dt'' \mathbf{l}(\mathbf{x}^s(t''))} \right)_{b'b''} f_{b''s}^0(\mathbf{x}^s(t)) \quad [\text{S20}]$$

so can be written as

$$\tilde{\mathcal{M}}_s(t) = \sum_b m_b(t) f_{bs}^0(\mathbf{x}^s(t)) \quad [\text{S21}]$$

with

$$m_b(t) = \int_0^t dt' \sum_{b'} c_{b'}(\mathbf{x}^s(t')) \left(e^{\int_{t'}^t dt'' \mathbf{l}(\mathbf{x}^s(t''))} \right)_{b'b} \quad [\text{S22}]$$

It is then straightforward to check that

$$\frac{d}{dt} m_b(t) = c_b(\mathbf{x}^s(t)) + \sum_{b'} m_{b'}(t) l_{b'b}(\mathbf{x}^s(t)) \quad [\text{S23}]$$

where the second term arises from the t -dependence of the matrix exponential. The $m_b(t)$ can therefore be obtained numerically by integrating the differential equations [S23] together with the subnetwork equations with (self-consistent) memory

$$\frac{d}{dt}x_s(t) = v_s(\mathbf{x}^s(t)) + \sum_{b'} m_{b'}(t) f_{sb'}^0(\mathbf{x}^s(t)) \quad [\text{S24}]$$

The appropriate initial conditions for the auxiliary variables follow from [S22] as $m_b(0) = 0$.

D Channel decomposition

We begin by writing the expression for the memory function explicitly, combining Eqs. [14, 18, 20, 21]:

$$M_s(\mathbf{x}^s, \tau) = \sum_{b's'b''} (\mathbf{J}^{-1})_{b'b''} \frac{\partial R_{b''}}{\partial x_{s'}} R_{s'} f_{b's}(\mathbf{x}^s, \tau) \quad [\text{S25}]$$

$$= \sum_{b's'b''} (\mathbf{J}^{-1})_{b'b''} \frac{\partial R_{b''}}{\partial x_{s'}} R_{s'} \sum_c E_{b''c}(\tau) f_{cs}^0(\phi_v(\mathbf{x}^s, \tau)) \quad [\text{S26}]$$

$$= \sum_{b's'b''} (\mathbf{J}^{-1})_{b'b''} \frac{\partial R_{b''}}{\partial x_{s'}} R_{s'} \sum_c E_{b''c}(\tau) \frac{\partial R_s}{\partial x_c}(\phi_v(\mathbf{x}^s, \tau)) \quad [\text{S27}]$$

where the first three factors are evaluated at \mathbf{x}^s . We now swap index labels and group the sums into a more intuitive form:

$$M_s(\mathbf{x}^s, \tau) = \sum_{s'} \sum_{bb'} \left(\sum_{b''} (\mathbf{J}^{-1})_{b''b'}(\mathbf{x}^s) \frac{\partial R_{b''}}{\partial x_{s'}}(\mathbf{x}^s) R_{s'}(\mathbf{x}^s) E_{b''b}(\tau) \frac{\partial R_s}{\partial x_b}(\phi_v(\mathbf{x}^s, \tau)) \right) \quad [\text{S28}]$$

As discussed in the main text, the expression up to before the exponential represents a change in the deviation of the bulk species concentration $x_{b''}$ from its QSS values over some small time interval, in response to changes in the subnetwork concentrations $x_{s'}$ (see also [S55] below). In the factor $\partial R_{b''}/\partial x_{s'}$ only those bulk species b'' contribute whose time evolution depends explicitly on the subnetwork species s' driving the bulk time evolution via $R_{s'}$. The b'' can then be interpreted as *outgoing channels* for the signal from s' . After propagation in the bulk network the signal returns via another bulk species. Here only bulk species b contribute that appear explicitly in the time evolution of subnetwork species s as indicated by the factors $\partial R_s/\partial x_b$. The b can therefore be interpreted as *incoming channels*. Overall, we have memory effects from s' onto s , via an outgoing channel (s' to b'') and an incoming channel (b to s). Consistent with this interpretation, the outgoing channel “susceptibilities” $\partial R_{b''}/\partial x_{s'}$ are evaluated for the past, i.e. “sending”, state $\mathbf{x}^s \equiv \mathbf{x}^s(t')$ of the subnetwork. The incoming channel susceptibilities $\partial R_s/\partial x_b$, on the other hand, are evaluated at the current time t as shown by the propagation via ϕ_v across the time difference $\tau = t - t'$. Within the self-consistent approximation [S23], this propagation corresponds directly to evaluation at the current state $\mathbf{x}^s(t)$.

E Self-consistent channel decomposition

The channel decomposition of Sec. C can also be applied to the self-consistent memory approximation, as we now outline. Writing out the self-consistent memory term [S20] explicitly and reordering and relabelling terms as in [S28] gives

$$\begin{aligned} \tilde{M}_s(t) &= \int_0^t dt' \sum_{s'} \sum_{bb'} \sum_{b''} \frac{\partial R_s}{\partial x_b}(\mathbf{x}^s(t)) \left(e^{\int_{t'}^t dt'' \mathbf{U}(\mathbf{x}^s(t''))} \right)_{b''b} (\mathbf{J}^{-1})_{b''b'}(\mathbf{x}^s(t')) \frac{\partial R_{b''}}{\partial x_{s'}}(\mathbf{x}^s(t')) R_{s'}(\mathbf{x}^s(t')) \quad [\text{S29}] \\ &= \sum_{s'} \sum_{bb'} \frac{\partial R_s}{\partial x_b}(\mathbf{x}^s(t)) m_{sbb's'}(t) \end{aligned}$$

where

$$m_{sbb's'}(t) = \int_0^t dt' \sum_{b''} (\mathbf{J}^{-1})_{b''b'}(\mathbf{x}^s(t')) \frac{\partial R_{b''}}{\partial x_{s'}}(\mathbf{x}^s(t')) R_{s'}(\mathbf{x}^s(t')) \left(e^{\int_{t'}^t dt'' \mathbf{U}(\mathbf{x}^s(t''))} \right)_{b''b} \quad [\text{S30}]$$

From this last representation it follows that the $m_{sbb's'}(t)$ vanish at $t = 0$ and obey the differential equations

$$\frac{d}{dt} m_{sbb's'}(t) = (\mathbf{J}^{-1})_{bb'}(\mathbf{x}^s(t)) \frac{\partial R_{b''}}{\partial x_{s'}}(\mathbf{x}^s(t)) R_{s'}(\mathbf{x}^s(t)) + \sum_{b''} m_{sbb'b''s'}(t) l_{b''b}(\mathbf{x}^s(t)) \quad [\text{S31}]$$

The channel-decomposed memory can therefore also be calculated from differential equations. Of course one only needs to find the $m_{sbb's'}$ for combinations (sb) and $(b's')$ where the corresponding channel susceptibilities are non-zero.

F Exactness of memory

We show that the self-consistent memory $m_b(t)$ is exact when both R_s and R_b contain at most linear terms in \mathbf{x}^b . In such a case, the full system can be written as

$$R_s = v_s + \sum_{b'} \tilde{x}_{b'} f_{b's}^0, \quad R_b = \sum_{b'} J_{bb'} \tilde{x}_{b'} \quad [S32]$$

where $\tilde{x}_b = x_b - x_b^*(\mathbf{x}^s)$ and the QSS value $\mathbf{x}^{b*}(\mathbf{x}^s)$ is an arbitrary function of \mathbf{x}^s . We now want to show that the \tilde{x}_b correspond *exactly* to the m_b from the self-consistent ZMs method. To do this we work out their evolution in time:

$$\frac{d}{dt} \tilde{x}_b = R_b - \sum_{s'} R_{s'} \frac{\partial x_b^*}{\partial x_{s'}} = \sum_{b'} J_{bb'} \tilde{x}_{b'} + \sum_{s'} \left(v_{s'} + \sum_{b'} \tilde{x}_{b'} f_{b's'}^0 \right) \sum_{b''} (\mathbf{J}^{-1})_{bb''} \frac{\partial R_{b''}}{\partial x_{s'}} \quad [S33]$$

By using that for an \mathbf{x}^b -linear system as assumed here one has $f_{bs}^0 = \partial R_s / \partial x_b$, the above can be rewritten as:

$$\frac{d}{dt} \tilde{x}_b = \sum_{b''} (\mathbf{J}^{-1})_{b'b''} \frac{\partial R_{b''}}{\partial x_{s'}} v_{s'} + \sum_{b'} \tilde{x}_{b'} \left(J_{b'b} + \sum_{s'b''} (\mathbf{J}^{-1})_{b'b''} \frac{\partial R_{b''}}{\partial x_{s'}} \frac{\partial R_{s'}}{\partial x_b} \right) \quad [S34]$$

Using then the definitions [16 & 21] we obtain an expression equivalent to [S23]

$$\frac{d}{dt} \tilde{x}_b = c_b + \sum_{b'} \tilde{x}_{b'} l_{b'b} \quad [S35]$$

thus showing that $\tilde{x}_b = m_b$ when we start from the same initial condition $\tilde{x}_b = 0$, *i.e.* the bulk at QSS.

We test the above exactness statement on two different examples that have a linear dependence on a particular species but nonlinear dependences on other species: a minimal bistable system as described in [Wilhelm, 2009], and the ‘‘Brusselator’’, which is capable of achieving limit cycles [Kondepudi and Prigogine, 1998]. As expected from the above derivation, the self-consistent memory captures the behaviour of both systems *exactly* (Fig. S1 & S2). As further shown in Fig S2, the original nonlinear projection method ZMn is also accurate at capturing the dynamics though not necessarily exact. (We note that the memory functions of the Brusselator grow exponentially in a way that forces memory terms to cancel out to zero at the fixed point; this leads to numerical challenges that we do not pursue here.)

G Linear dynamics

We discuss briefly the case of fully linear dynamics, where the dependence of R_s and R_b on *all* variables \mathbf{x}^s and \mathbf{x}^b (not just \mathbf{x}^b as in Supp. F) is only via constant and linear terms. Such a description can always be obtained by expanding linearly around a fixed point of the dynamics [Rubin et al., 2014, Herrera-Delgado et al., 2018]. One then sees from [16] and [14] that $l_{bb'}$ and f_{bs}^0 are both constant, *i.e.* independent of \mathbf{x}^s . Accordingly (compare [18, 20] and [24]) also the memory functions of the ZMn and ZMs projections become identical, and the corresponding channel decompositions are also the same.

To illustrate the linearised dynamics approach, we perform a channel decomposition of the amplitude (value at $\tau = 0$) of the linearised memory in the neural tube system as we did in [Herrera-Delgado et al., 2018], but now for the method derived in this study (Fig. S4). We find similar profiles to those found in [Herrera-Delgado et al., 2018]. The results highlight the relative weakness of the memory from Olig2 into Nkx2.2 via Pax6, supporting the conclusions of [Herrera-Delgado et al., 2018]. The method derived in this study is, however, significantly more powerful as it does not rely on an expansion near a steady state and gives access to the full memory and its channel decomposition as described in Supp. D & E.

H Comparison with alternative memory function approximation

Gouasmi *et al* [Gouasmi et al., 2017] propose an approximation for the memory function for the case where the projection [10] is defined not by setting the bulk coordinates to their \mathbf{x}^s -dependent QSS values, but simply to zero:

$$E[g(\cdot)|\mathbf{x}^s] = g(\mathbf{x}^s, 0) \quad [S36]$$

The function $F_s(\mathbf{x}^s, \mathbf{x}^b, \tau)$ still evolves according to [5], which written out now reads

$$\frac{\partial}{\partial \tau} F_s = L F_s(\mathbf{x}^s, \mathbf{x}^b, \tau) - E[L F_s(\cdot, \tau)|\mathbf{x}^s] \quad [S37]$$

$$\begin{aligned} &= \sum_{s'} R_{s'}(\mathbf{x}^s, \mathbf{x}^b) \frac{\partial F_s}{\partial x_{s'}} + \sum_b R_b(\mathbf{x}^s, \mathbf{x}^b) \frac{\partial F_s}{\partial x_b} \\ &\quad - \sum_{s'} R_{s'}(\mathbf{x}^s, 0) \frac{\partial F_s}{\partial x_{s'}}(\mathbf{x}^s, 0, \tau) - \sum_b R_b(\mathbf{x}^s, 0) \frac{\partial F_s}{\partial x_b}(\mathbf{x}^s, 0, \tau) \end{aligned} \quad [S38]$$

where the very last factor is the x_b -derivative of F evaluated at $\mathbf{x}^b = 0$. The approximation of [Gouasmi et al., 2017] amounts to ignoring the fact that the derivatives of F_s are evaluated at a different point in the second line, which gives

$$\frac{\partial}{\partial \tau} F_s = \sum_{s'} [R_{s'}(\mathbf{x}^s, \mathbf{x}^b) - R_{s'}(\mathbf{x}^s, 0)] \frac{\partial F_s}{\partial x_{s'}} + \sum_b [R_b(\mathbf{x}^s, \mathbf{x}^b) - R_b(\mathbf{x}^s, 0)] \frac{\partial F_s}{\partial x_b} \quad [S39]$$

This has the form of a Liouville equation as noticed in [Gouasmi et al., 2017] and so its solution can be written as

$$F_s(\mathbf{x}^s, \mathbf{x}^b, \tau) = F_s(\boldsymbol{\psi}^s(\mathbf{x}^s, \mathbf{x}^b, \tau), \boldsymbol{\psi}^b(\mathbf{x}^s, \mathbf{x}^b, \tau)) \quad [S40]$$

where the components of the vector functions $\boldsymbol{\psi}^s$ and $\boldsymbol{\psi}^b$ evolve with τ according to

$$\frac{\partial}{\partial \tau} \psi_s = R_s(\boldsymbol{\psi}^s, \boldsymbol{\psi}^b) - R_s(\boldsymbol{\psi}^s, 0) \quad [S41]$$

$$\frac{\partial}{\partial \tau} \psi_b = R_b(\boldsymbol{\psi}^s, \boldsymbol{\psi}^b) - R_b(\boldsymbol{\psi}^s, 0) \quad [S42]$$

from the initial conditions

$$\psi_b(\mathbf{x}^s, \mathbf{x}^b, 0) = x_b, \quad \psi_s(\mathbf{x}^s, \mathbf{x}^b, 0) = x_s \quad [S43]$$

The function F_s at $\tau = 0$, which as before we write without a time argument, is given by the analogue of [12],

$$F_s(\mathbf{x}^s, \mathbf{x}^b) = R_s(\mathbf{x}^s, \mathbf{x}^b) - R_s(\mathbf{x}^s, 0) \quad [S44]$$

The corresponding memory as defined in [19] is

$$M_s^G(\mathbf{x}^s, \tau) = \sum_{s'} R_{s'} \frac{\partial}{\partial x_{s'}} F_s(\boldsymbol{\psi}^s, \boldsymbol{\psi}^b) + \sum_b R_b \frac{\partial}{\partial x_b} F(\boldsymbol{\psi}^s, \boldsymbol{\psi}^b) \quad [S45]$$

where all $R_{s'}$, R_b and the derivatives are evaluated at $(\mathbf{x}^s, 0)$. Gouasmi *et al* propose to find these derivatives numerically, but in fact a closed form expression can be obtained, as follows. Applying the chain rule gives

$$M_s^G(\mathbf{x}^s, \tau) = \sum_{s's''} R_{s'} \frac{\partial F_s}{\partial \psi_{s''}} \frac{\partial \psi_{s''}}{\partial x_{s'}} + \sum_{s'b} R_{s'} \frac{\partial F_s}{\partial \psi_b} \frac{\partial \psi_b}{\partial x_{s'}} + \sum_{s'b} R_b \frac{\partial F_s}{\partial \psi_{s'}} \frac{\partial \psi_{s'}}{\partial x_b} + \sum_{bb'} R_b \frac{\partial F_s}{\partial \psi_{b'}} \frac{\partial \psi_{b'}}{\partial x_b} \quad [S46]$$

Now note that in the final evaluation we always use $\mathbf{x}^b = 0$, which from the differential equations [S41, S42] implies $\boldsymbol{\psi}^s = \mathbf{x}^s$, $\boldsymbol{\psi}^b = 0$ for all τ . Hence in particular ψ_b is independent of \mathbf{x}^s and so $\partial \psi_b / \partial x_{s'} = 0$. We also have $F_s(\mathbf{x}^s, 0) = 0$ from [S44], which implies $\partial F_s / \partial \psi_{s'} = 0$. Only the last term from [S46] thus survives:

$$M^G(\mathbf{x}^s, \tau) = \sum_{bb'} R_b \frac{\partial F_s}{\partial \psi_{b'}} \frac{\partial \psi_{b'}}{\partial x_b} \quad [S47]$$

and it remains to find $\partial \psi_{b'} / \partial x_b$. By differentiating [S42] for $\partial \psi_{b'} / \partial \tau$ w.r.t. x_b one finds

$$\frac{\partial}{\partial \tau} \frac{\partial \psi_{b'}}{\partial x_b} = \frac{\partial R_{b'}}{\partial \psi_{b''}} \frac{\partial \psi_{b''}}{\partial x_b} \quad [S48]$$

On the r.h.s. a similar term from the variation of $\boldsymbol{\psi}^s$ vanishes as it would be proportional to

$$\frac{\partial R_{b'}}{\partial \psi_s}(\boldsymbol{\psi}^s, \boldsymbol{\psi}^b) - \frac{\partial R_{b'}}{\partial \psi_s}(\boldsymbol{\psi}^s, 0) \quad [S49]$$

This difference is zero in the final evaluation at $\mathbf{x}^b = 0$ (which implies $\boldsymbol{\psi}^b = 0$). For the same reason the derivatives $\partial R_{b'} / \partial \psi_{b''} = \partial R_{b'} / \partial x_{b''}$ are evaluated at $(\mathbf{x}^s, 0)$ and constant in time τ . Collecting these derivatives into a matrix \mathbf{k} with elements $k_{b'b''}$ and using that $\partial \psi_{b''} / \partial x_b = \delta_{bb''}$ ($= 1$ for $b = b''$ and $= 0$ otherwise) at $\tau = 0$ gives then as the explicit solution of [S48]

$$\frac{\partial \psi_{b'}}{\partial x_b} = (e^{\mathbf{k}\tau})_{b'b} \quad [S50]$$

and inserting into [S47] yields

$$M^G(\mathbf{x}^s, \tau) = \sum_{bb'} \frac{\partial R_s}{\partial x_{b'}} (e^{\mathbf{k}\tau})_{b'b} R_b \quad [S51]$$

where we have used that $\partial F_s / \partial \psi_{b'} = \partial F_s / \partial x_{b'} = \partial R_s / \partial x_{b'}$; this derivative and the factor R_b are evaluated at $(\mathbf{x}^s, 0)$ in the approximation from [Gouasmi et al., 2017] for the memory function.

We do not show here how the above memory approximation performs in our test systems because the nature of the approach can lead to fixed points disappearing after projection or new fixed points appearing. We observed both of these effects in numerical evaluations for the bistable switch from [Wilhelm, 2009].

I Extending Gouasmi *et al* approximation with QSS projection

The Gouasmi *et al.* approximation [Gouasmi et al., 2017] for the memory function rests on projecting to $\mathbf{x}^b = 0$, but this is not generally an appropriate baseline for our case as it would correspond to setting all bulk concentrations to zero. However, we can adapt the approximation to the spirit of our work by changing coordinate system so that zero bulk coordinates correspond to the projection we consider throughout the paper, i.e. to QSS bulk concentrations. Explicitly, this variable transformation reads

$$\tilde{x}_s = x_s, \quad \tilde{x}_b = x_b - x_b^*(\mathbf{x}^s) \quad [\text{S52}]$$

because $\tilde{x}_b = 0$ is then equivalent to $x_b = x_b^*(\mathbf{x}^s)$. The time evolution of the new variables follows as

$$\frac{d}{dt}\tilde{x}_s = \tilde{R}_s(\tilde{\mathbf{x}}^s, \tilde{\mathbf{x}}^b) = R_s(\tilde{\mathbf{x}}^s, \mathbf{x}^{b*} + \tilde{\mathbf{x}}^b) \quad [\text{S53}]$$

$$\frac{d}{dt}\tilde{x}_b = \tilde{R}_b(\tilde{\mathbf{x}}^s, \tilde{\mathbf{x}}^b) \quad [\text{S54}]$$

$$= R_b(\tilde{\mathbf{x}}^s, \mathbf{x}^{b*} + \tilde{\mathbf{x}}^b) + \sum_s \left[\sum_{b'} (\mathbf{J}^{-1})_{bb'} \frac{\partial R_{b'}}{\partial x_s} \right] R_s(\tilde{\mathbf{x}}^s, \mathbf{x}^{b*} + \tilde{\mathbf{x}}^b) \quad [\text{S55}]$$

where the factors enclosed in square brackets are the explicit expression for $-\partial x_b^*/\partial x_s$ and have to be evaluated at \mathbf{x}^{b*} .

The Gouasmi memory function approximation, adapted for our QSS projection, is now given by [S51] applied to the new variables \tilde{x}_s, \tilde{x}_b and corresponding drift functions \tilde{R}_s, \tilde{R}_b . The last factor is $\tilde{R}_b(\tilde{\mathbf{x}}^s, 0)$, which can be read off from [S55]. The first term in [S55] vanishes as $R_b = 0$ at QSS, while the remainder is seen to be precisely $c_b(\mathbf{x}^s)$ from [21]. The matrix \mathbf{k} in the new variables has elements

$$k_{b'b} = \frac{\partial \tilde{R}_{b'}}{\partial \tilde{x}_b} = \frac{\partial R_{b'}}{\partial x_b} + \sum_s \left[\sum_{b'} (\mathbf{J}^{-1})_{bb'} \frac{\partial R_{b'}}{\partial x_s} \right] \frac{\partial R_s}{\partial x_b} = l_{bb'} \quad [\text{S56}]$$

Note that the terms in square brackets are already just dependent on \mathbf{x}^s , so do not contribute to the derivative. The remaining factor in the memory function is, again in the new variables,

$$\frac{\partial \tilde{R}_s}{\partial \tilde{x}_{b'}} = \frac{\partial R_s}{\partial x_{b'}} \quad [\text{S57}]$$

so that overall

$$\tilde{M}_s^G(\mathbf{x}^s, \tau) = \sum_{bb'} \frac{\partial R_s}{\partial x_{b'}} (e^{l(\mathbf{x}^s)\tau})_{bb'} c_b(\mathbf{x}^s) = \sum_{b'} c_{b'}(\mathbf{x}^s) \tilde{f}_{b's}(\mathbf{x}^s, \tau) \quad [\text{S58}]$$

with

$$\tilde{f}_{b's}(\mathbf{x}^s, \tau) = \left(e^{l(\mathbf{x}^s)\tau} \right)_{b'b} f_{bs}^0(\mathbf{x}^s) \quad [\text{S59}]$$

where we have used the definition of f_{bs}^0 from [14]. Comparing now [18] and [S59] shows that the memory approximation [S58], though derived here from rather different arguments, is quite similar to our expression [20]: the only difference is that the propagation from \mathbf{x}^s to $\phi_v(\mathbf{x}^s, \tau)$ is absent in $\tilde{f}_{b's}$, which is the analogue of our f_{bs} . We show that without the ϕ_v -propagation the method can still perform accurately in some situations but breaks down in other settings (Fig. S2).

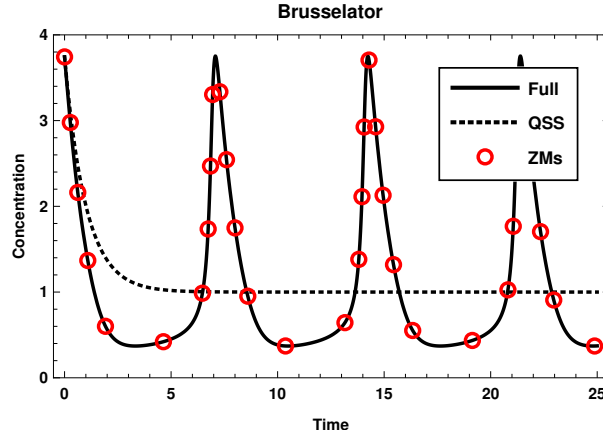


Figure S1: Oscillating Brusselator system as described in [Kondepudi and Prigogine, 1998]; we retain the concentration of the first species x_1 in the subnetwork and place the second species in the bulk. Parameters for the sustained oscillatory regime in this example are $A = 1$ and $B = 3$ in the notation of [Kondepudi and Prigogine, 1998]. The trajectory of the self-consistent projection (red dots) captures that of the original system (solid line) exactly as expected from the general proof in Supp. F, while the QSS (dotted line) fails qualitatively.

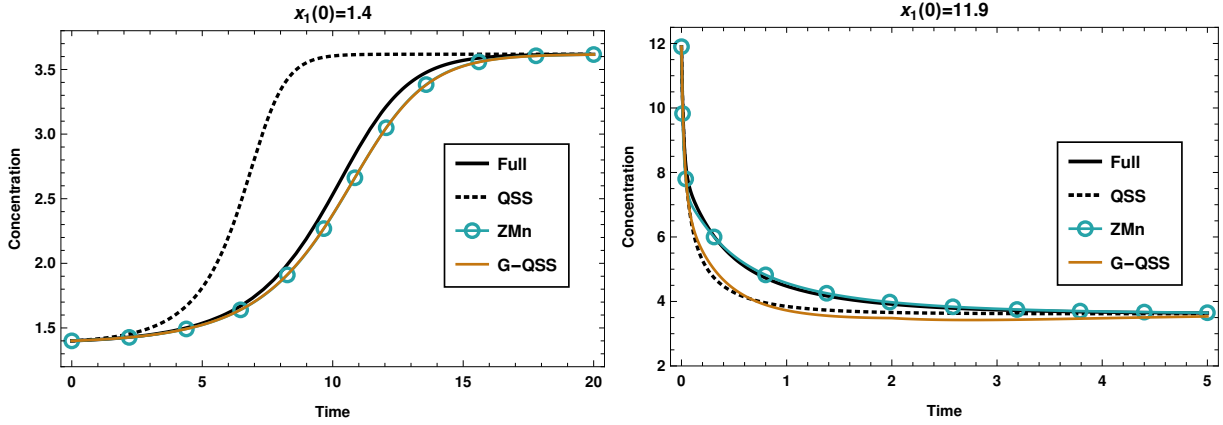


Figure S2: Minimal bistable system with linear dependence on the second species as described in [Wilhelm, 2009]; we choose x_1 for the subnetwork and place the second species in the bulk. Parameters for the bistable regime in this example are: $k_1 = 10$, $k_2 = 1$, $k_3 = 2$ and $k_4 = 1$ [Wilhelm, 2009]. The trajectory of the self-consistent ZMs projection again captures that of the original system (solid line) exactly (see Supp. F & Fig. S1) so is not plotted. G-QSS represents the Gouasmi *et al.* approach adapted to QSS projection (Supp. I). (Left) At initial conditions near the fixed point both the ZMn method (cyan dots) and G-QSS (orange line) behave similarly and accurately capture the full dynamics. (Right) Further away from the final stable fixed point the G-QSS predictions become increasingly inaccurate while the ZMn method continues to provide a good approximation.

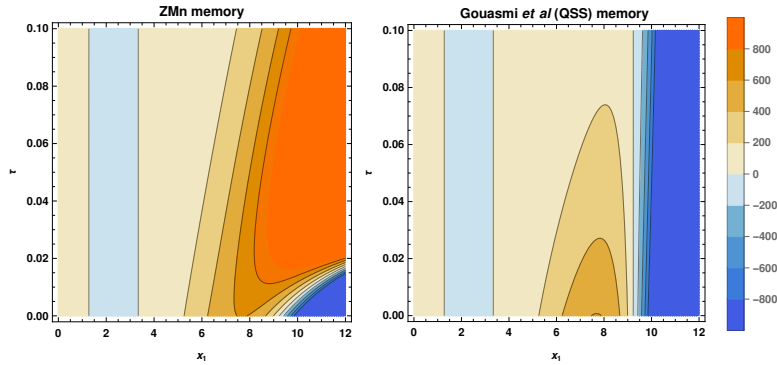


Figure S3: Memory functions for the system detailed in [Wilhelm, 2009] with the parameters chosen for Fig. S2, using the ZMn (left) and the method from Gouasmi *et al.* as extended to QSS projection in Supp. I (right). The x -axis shows the concentration of the subnetwork species x_1 while the y -axis indicates time difference τ . By construction, the two memory function approximations predict the same value (scale bar to the right) at $\tau = 0$, as they only differ in how they propagate the memory over time. At $\tau > 0$ the memory functions are relatively similar for $x_1 \in [0, 6]$ but become progressively different as x_1 grows beyond this range; for $x_1 \geq 10$ the G-QSS method predicts a negative memory function for all τ that leads to its poor performance as observed in Fig. S2.

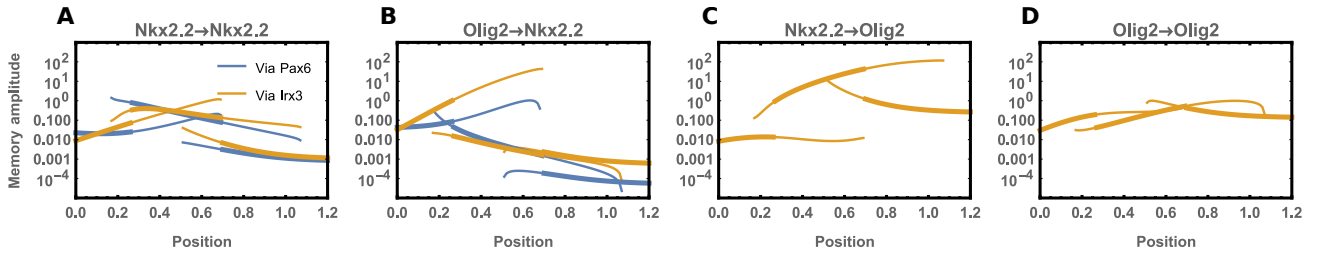


Figure S4: Amplitudes (value at time difference $\tau = 0$) of nonlinear memory functions linearised around fixed points, for comparison with the approach of [Herrera-Delgado et al., 2018], where memory functions expanded around fixed points were calculated directly. (A) Amplitude of memory of Nkx2.2 to itself along the neural tube. There are multiple lines as the analysis was performed at all possible stable steady states. The vertical axis is logarithmic to make the range of amplitudes easier to appreciate. Colours identify the memory amplitude contribution from the two possible bulk channels, via Irx3 and Pax6, respectively. Thick lines indicate physiological states, while thin lines indicate states that are not usually observed in vivo. (B) Amplitude of memory of Nkx2.2 to levels of Olig2, shown along the neural tube. The memory via Pax6 is for the most part below the memory via Irx3, in each pair of corresponding curves. (C,D) Amplitudes of memory of Olig2 to past Nkx2.2 (C) and to itself (D). No channel decomposition is performed as Olig2 receives memory only via the Irx3 channel.

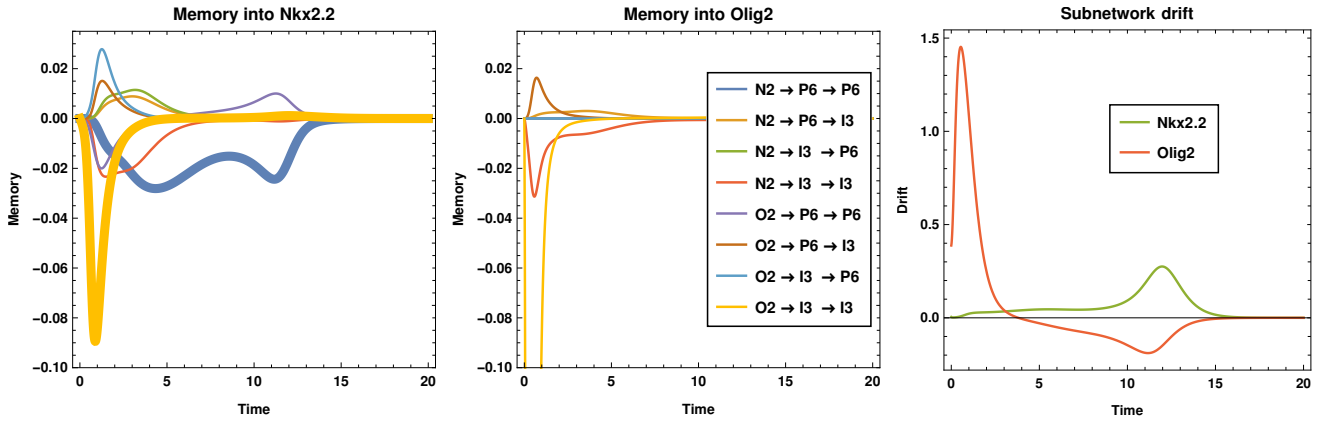


Figure S5: Channel decomposition of the memory terms for the ZMs trajectory shown in Fig. 6. Left and centre show memory terms affecting Nkx2.2 and Olig2 respectively. Each colour represents a memory channel as indicated. The memory originates from a particular subnetwork species “sending” memory through a specific bulk species; the effect then propagates within the bulk and returns via a specific bulk species (see legend). The two most salient memory functions are: Nkx2.2 to Pax6 and then returning through Pax6 into Nkx2.2 (thick yellow line), and Olig2 to Irx3 and then returning through Pax6 into Nkx2.2 (thick blue line). The centre plot shows a large memory contribution acting on Olig2 via the channel through Irx3 (yellow line). However, in this case the drift for Olig2 (right panel) is so large that the relative effect of this memory channel remains nonetheless small.